Robotica (2009) volume 27, pp. 763–770. © 2008 Cambridge University Press
doi:10.1017/S0263574708005213 Printed in the United Kingdom

Object exploration and manipulation using a robotic finger equipped with an optical three-axis tactile sensor

Masahiro Ohka*†, Jumpei Takata‡, Hiroaki Kobayashi§, Hirofumi Suzuki¶, Nobuyuki Morisawa‖ and Hanafiah Bin Yussof†‡‡

†*Department of Complex Systems Science, Graduate School of Information Science, Nagoya University, Furo-cho, Chikusa-ku, Nagoya, 464-8601, Japan*
‡*Olympus Corporation, 2-3-1 Nishi-shinzyuku-ku, Tokyo 163-0914, Japan*
§*Toyota Industry Corporation, 2-1 Toyoda-cho, Kariya 448-8671, Japan*
‖*Department of Electronic Mechanical Engineering, Graduate School of Engineering, Nagoya University, Furo-cho, Chikusa-ku, Nagoya, 464-8601, Japan*
¶ *Honda R & D Co. Ltd., 1-4-1 Chuo, Wako-shi, Saitama-ken 351-0193, Japan*
‡‡*Universiti Teknologi MARA, 40450 Shah Alam, Selangor, Malaysia*

(Received in Final Form: October 21, 2008. First published online: November 17, 2008)

SUMMARY
To evaluate our three-axis tactile sensor developed in preceding papers, a tactile sensor is mounted on a robotic finger with 3-degrees of freedom. We develop a dual computer system that possesses two computers to enhance processing speed: one is for tactile information processing and the other controls the robotic finger; these computers are connected to a local area network. Three kinds of experiments are performed to evaluate the robotic finger's basic abilities required for dexterous hands. First, the robotic hand touches and scans flat specimens to evaluate their surface condition. Second, it detects objects with parallelepiped and cylindrical contours. Finally, it manipulates a parallelepiped object put on a table by sliding it. Since the present robotic hand performed the above three tasks, we conclude that it is applicable to the dexterous hand in subsequent studies.

KEYWORDS: Tactile sensor; Three-axis; Surface measurement; Contour measurement; Object manipulation; Robotic finger.

1. Introduction

Since three-axis tactile sensors can simultaneously detect normal and shearing forces, their sensing ability is superior to other tactile sensors[1–5] and can detect the contact physics between an object and a finger surface. They can also provide tactile information for material handling.[6,7] Since flexible and impact resistant surfaces are the most important, we improved conventional optical waveguide-type tactile sensors[8–12] and developed an optical three-axis tactile sensor.[13,14]

In previous papers[15,16] subsequent to our work,[13,14] we developed a hemispherical tactile sensor for general-purpose use with our three-axis tactile sensor to mount on the fingertips of a multifingered hand. When we examined the repeatability of the present tactile sensor with 1,000 load/unload cycles, the respective error of the normal and shearing forces was 2 and 5% for evaluating the basic characteristics needed for application to robotic dexterous hands.

On the other hand, so far several researchers have mounted tactile sensors on robotic multifingered hands to enhance manipulation and stable grasping abilities. Kaneko *et al.*[11] and Maekawa *et al.*[12] formulated dynamics including tactile information obtained by conventional optical waveguide-type tactile sensors mounted on fingertips. These studies are considered important milestones because they showed the effectiveness of tactile information on multifingered hands.

If the three-axis tactile sensor is used instead of the conventional tactile sensor, robotic hand can obtain the differences in an object's attitude, friction coefficient, and the subtle unevenness of its surface. Therefore, application will increase by equipment that uses three-axis tactile sensors. Humanoid robots must be able to grasp slippery or flexible objects, especially in living environments with human beings, in contrast to industrial robots that handle standardized objects in controlled environments. Since the three-axis tactile sensor is effective in such cases, its importance will increase with improvements of humanoid robots.

In this paper, we discuss a robotic finger equipped with the three-axis tactile sensor that was developed in our previous study[16,17] as the first step in a series of studies for a dexterous multifingered hand. Our present robotic hand possesses three motorized joints and a three-axis tactile sensor on each fingertip. To exploit the present results for the multifingered hand in subsequent studies, we performed experiments on such basic motions as surface scanning and object manipulation that we performed in object recognition and stable grasping.

2. Three-axis Tactile Sensor

Figure 1 shows a schematic view of the present tactile processing system to explain its sensing principle. The present tactile sensor is composed of a CCD camera, an acrylic board, a light source, and a computer. The light emitted from the light source is directed into the optical

*Corresponding author. E-mail: ohka@is.nagoya-u.ac.jp

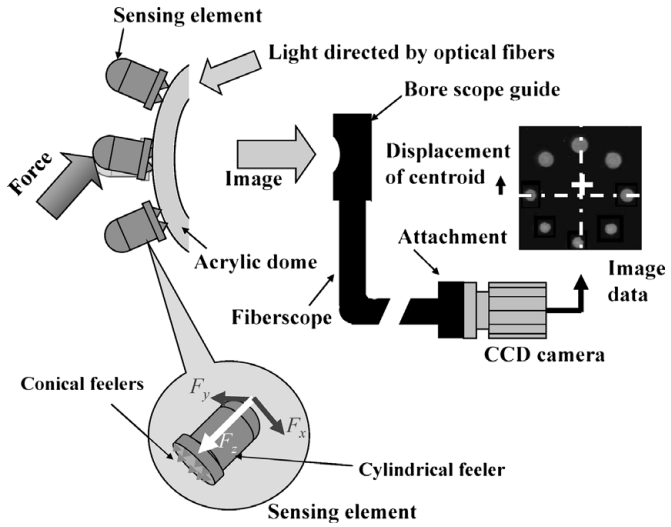

Fig. 1. Principle of three-axis tactile sensor.

waveguide dome. Contact phenomena are observed as image data, acquired by the CCD camera, and transmitted to the computer to calculate the three-axis force distribution.

The sensing element presented in this paper is comprised of a columnar feeler and eight conical feelers, as shown in Fig. 1. The sensing elements, made of silicone rubber, are designed to maintain contact with the conical feelers and the acrylic dome so that the columnar feelers touch an object. Each columnar feeler fit the flange into a counter bore portion in the fixing dome to protect the columnar feeler from horizontal displacement caused by shearing force.

When the three components of a force vector, F_x, F_y, and F_z, are applied to the tip of the columnar feeler, contact between the acrylic dome and the conical feelers is measured as a distribution of gray-scale values that are transmitted to the computer. The F_x, F_y, and F_z values are calculated using integrated gray-scale value G and horizontal displacement of the centroid of gray-scale distribution $\boldsymbol{u} = u_x\mathbf{i} + u_y\mathbf{j}$ as follows:

$$F_x = f(u_x), \tag{1}$$

$$F_y = f(u_y), \tag{2}$$

$$F_z = g(G), \tag{3}$$

where $\mathbf{i}$ and $\mathbf{j}$ are the orthogonal base vectors of the x- and y-axes of a Cartesian coordinate attached to the base of the sensing element, respectively; $f(x)$ and $g(x)$ are approximate curves estimated in calibration experiments.

Since the tactile sensors must be fitted to a multifingered hand, we are developing a fingertip to include a hemispherical three-axis tactile sensor in which the fingertip and the three-axis tactile sensor are united, as shown in Fig. 2. The sensing elements are concentrically arranged on an acrylic dome that is illuminated along its edge by optical fibers connected to a light source. Image data consisting of bright spots caused by the feelers' collapse are retrieved by an optical fiberscope connected to the CCD camera.

3. Dual Computer System

Since the present tactile sensor is based on image processing that requires heavy calculation time, we only use a computer to process image data acquired by the CCD camera. Toward a dexterous robotic hand equipped with the present tactile sensors, as shown in Fig. 3, we have tentatively developed a system of a robotic finger system that possesses two computers; one is for tactile information processing; the other is for controlling the robotic finger; these computers are connected to a local area network.

Image data acquired by the CCD camera are divided into 41 subregions, as shown in the tactile sensor system on the right of Fig. 3. The dividing procedure, digital filtering, integrated gray-scale value, and centroid displacement are processed on the image processing board. Since the image warps due to projection from a hemispherical surface, software installed on the computer modifies the warped image data and calculates G, u_x, and u_y to obtain the three-axis force applied to the tip of the sensing element using Eqs. (1)–(3).

On the left of Fig. 3, a robotic finger system is shown that is comprised of a robotic finger, a motor drive, a digital I/O board, and another computer. The robotic finger includes links, fingertips equipped with the three-axis tactile sensor,

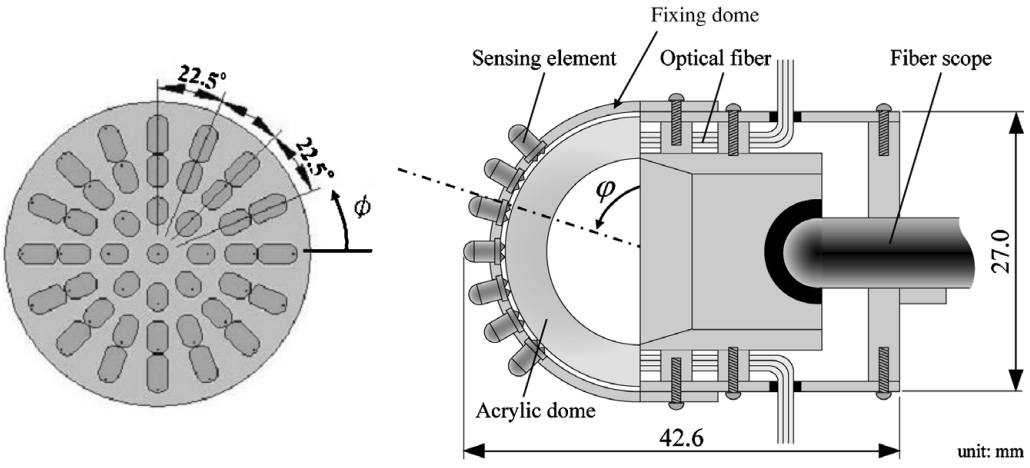

Fig. 2. Fingertip including three-axis tactile sensor.

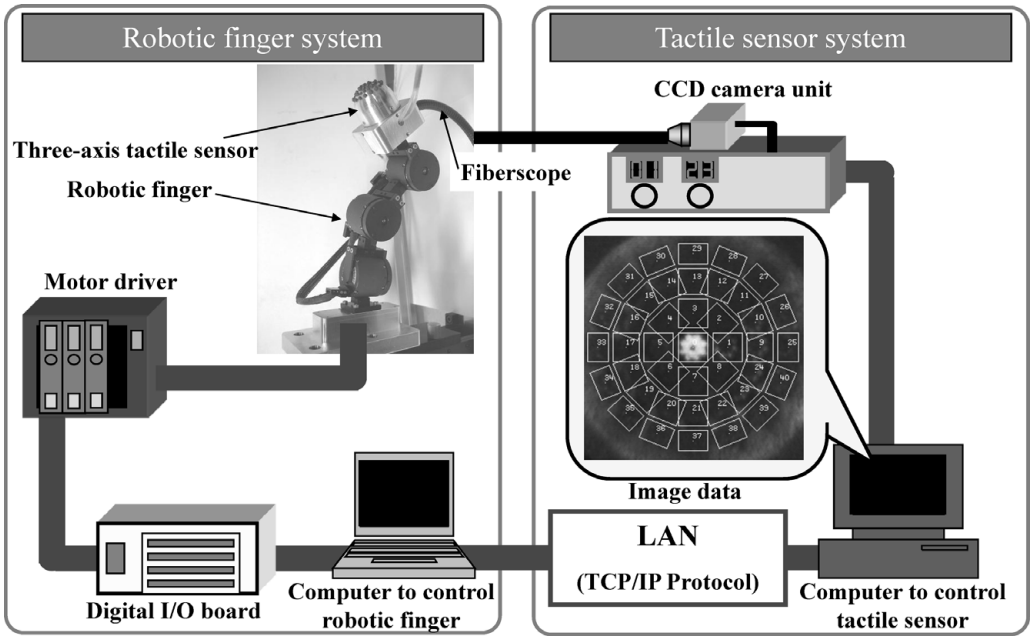

Fig. 3. Overview of the present system.

and micro actuators (YR-KA01-A000, Yasukawa) which are used in every movable joint, that consist of a micro-AC servo motor, a harmonic gear (reduction ratio: 1/80, maximum torque: 0.7 Nm), and a digital encoder.

After tactile data are obtained by the above process, they are sent to the computer for robotic finger control through the local area network. In the computer, signals applied to the joint motors of the robotic finger are calculated so that the fingertip follows a trajectory based on an algorithm called resolved motion rate control described in the next section. The signals are sent to the motor driver through the digital I/O board to drive the micro actuators.

4. Resolved Motion Rate Control

As shown in Fig. 4, the present robotic finger has three movable joints. The kinematics of the present hand is derived based on the Denabit–Hartenberg notation shown in Fig. 4. The frame of the workspace is set on the bottom of the z-stage and defined as O-xyz. The frames of Oi$-x_i y_i z_i (i = 0, 2, \ldots, 5)$ (in the following, O-xyz is used instead of $O_0-x_0y_0z_0$) are attached to each joint, the basement of the z-stage, or the fingertip. The velocities of the micro actuators ($\dot{\boldsymbol{\theta}} = (\dot{\theta}_1\ \dot{\theta}_2\ \dot{\theta}_3)$) are calculated with

$$\dot{\boldsymbol{\theta}} = \boldsymbol{J}^{-1}(\boldsymbol{\theta})\dot{\mathbf{r}} \tag{4}$$

to satisfy specified velocity vector $\dot{\mathbf{r}}(= (\dot{x}\ \dot{y}\ \dot{z}))$, which is calculated from the planed trajectory. Jacobian $\boldsymbol{J}(\boldsymbol{\theta})$ is obtained by the kinematics of the robotic hand as follows:

$$\begin{aligned}\boldsymbol{J}(\boldsymbol{\theta}) &= \begin{bmatrix} -R_{13}(l_2+l_3c_2+l_4c_{23})\ l_3(R_{11}s_3+R_{12}c_3)+l_4R_{12}\ R_{12}l_4 \\ -R_{23}(l_2+l_3c_2+l_4c_{23})\ l_3(R_{21}s_3+R_{22}c_3)+l_4R_{22}\ R_{22}l_4 \\ -R_{33}(l_2+l_3c_2+l_4c_{23})\ l_3(R_{31}s_3+R_{32}c_3)+l_4R_{32}\ R_{32}l_4 \end{bmatrix}, \\ \begin{bmatrix} R_{11} & R_{12} & R_{13} \\ R_{21} & R_{22} & R_{23} \\ R_{31} & R_{32} & R_{33} \end{bmatrix} &= \begin{bmatrix} a_{11}c_{23}+a_{13}s_{23} & -a_{11}s_{23}+a_{13}c_{23} & -a_{12} \\ a_{21}c_{23}+a_{23}s_{23} & -a_{21}s_{23}+a_{23}c_{23} & -a_{22} \\ a_{31}c_{23}+a_{33}s_{23} & -a_{31}s_{23}+a_{33}c_{33} & -a_{32} \end{bmatrix}, \\ \begin{bmatrix} a_{11} & a_{12} & a_{13} \\ a_{21} & a_{22} & a_{23} \\ a_{31} & a_{32} & a_{33} \end{bmatrix} &= \begin{bmatrix} c\phi_1c_1+s\phi_1s\phi_2s_1 & -c\phi_1s_1+s\phi_1s\phi_2s_1 & s\phi_1c\phi_2 \\ c\phi_2s\phi_1 & c\phi_2s\phi_1 & -s\phi_2 \\ -s\phi_1c_1+s\phi_1s\phi_2s_1 & s\phi_1s_1+c\phi_1s\phi_2c\phi_1 & c\phi_1c\phi_2 \end{bmatrix} \end{aligned} \tag{5, 6}$$

where

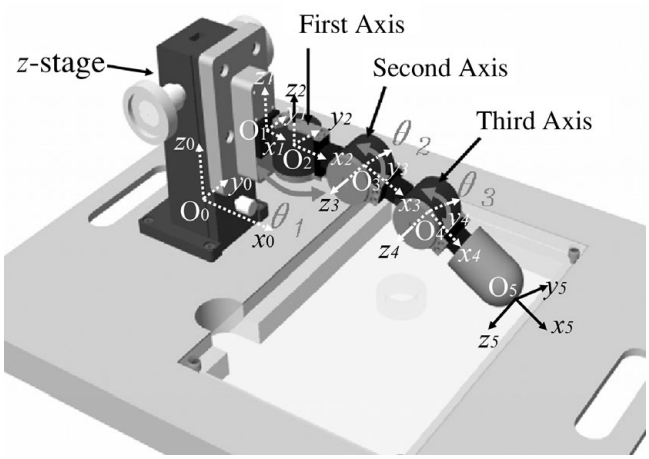

Fig. 4. Robotic finger equipped with a three-axis tactile sensor.

$$c_i \equiv \cos\theta_i, s_i \equiv \sin\theta_i, c\phi_i \equiv \cos\phi_i, s\phi_i \equiv \sin\phi_i,$$
$$c_{ij} \equiv \cos(\theta_i + \theta_j), s_{ij} \equiv \sin(\theta_i + \theta_j), (i; j = 1, 2, 3).$$

In the above equations, the rotations of the first frame around the x_0- and y_0-axes are denoted as ϕ_1 and ϕ_2, respectively. The distance between the origins of the mth and $m+1$th frames is denoted as l_m. The joint angles of the micro actuators are θ_1, θ_2, and θ_3 (Fig. 4).

Position control of the fingertip is performed based on resolved motion rate control,[18,19] in which joint angles are assumed in the first step, and displacement vector $\mathbf{r}_0$is calculated with kinematics. Adjustment of the joint angles is obtained by Eq. (4) and the difference between $\mathbf{r}_0$ and objective vector $\mathbf{r}_d$ to modify joint angle $\boldsymbol{\theta}_1$ in the next step. The modified joint angle is designated as the current angle in the next step, and the above procedure is repeated until the displacement vector at kth step $\mathbf{r}_k$ coincides with objective vector $\mathbf{r}_d$ within a specified error. That is, Eqs. (7) and (8) are calculated until $|\mathbf{r}_d - \mathbf{r}_k|$ becomes small enough:

$$\dot{\mathbf{r}}_k = J\dot{\boldsymbol{\theta}}_k \tag{7}$$
$$\boldsymbol{\theta}_{k+1} = \boldsymbol{\theta}_k - \boldsymbol{J}^{-1}(\mathbf{r}_d - \mathbf{r}_k) \tag{8}$$

5. Evaluation Experiments

5.1. Scanning on flat surfaces

In subsequent studies, we will develop a multifingered hand composed of the present robotic finger and perform object recognition and manipulation tests using the hand. To exploit the present results for the multifingered hand in subsequent studies, we perform experiments on such basic motions as surface scanning and object manipulation.

First, in scanning on a flat surface, a sensing element located on the vertex of the tactile sensor makes perpendicular contact with a flat table by adjusting angles θ_2 and θ_3. After that, a z-stage equipped with a robotic finger is adjusted to obtain appropriate contact force (0.1 N). Precision abrasive paper (produced by Sumitomo 3M) is mounted on the table. In this experiment, three kinds of abrasive paper, 1, 30, and 60 μm, were adopted as specimens. To examine the dependence of friction coefficient on scanning speed, we chose three speeds: 1.4, 6.2, and 25 mm/sec.

5.2. Contour tracing

In contour tracing, the robotic finger moves linearly and traces the object contour after touching it (Fig. 5). Functions are shared among sensing elements to realize this behavior with a simple algorithm. In this experiment, the robotic finger seeks the table with a linear downward motion before the contour-tracing mode. If the sensing element accepts the normal force that exceeded 0.2 N, the robotic finger judges that it has reached the table and designates the element and the neighboring elements as a table detector. After finding the table, the robotic finger moves 5 mm up and switches to the contour-tracing mode. Since the fingertip orientation maintains a perpendicular direction to the table, sensing elements touch the object contour, except for the element and the neighboring elements.

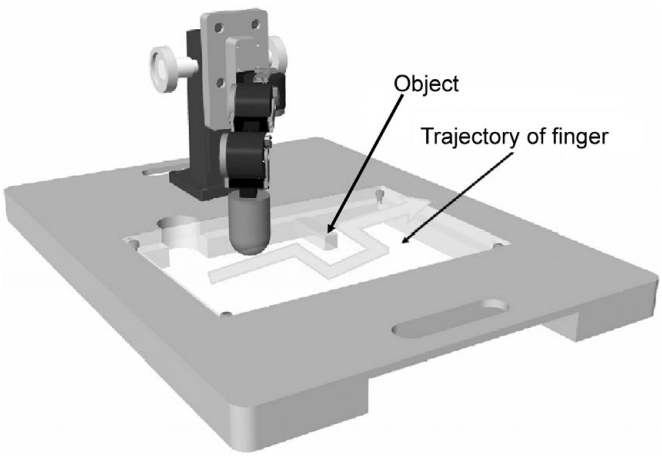

Fig. 5. Contour detection test.

During the contour-tracing mode, if one of the sensing elements accepts normal force that exceeded 0.3 N, the robotic finger comes off the object's side surface and moves 5 mm from the surface. Then it moves linearly 5 mm in a direction perpendicularly intersecting the coming-off direction. Then it approaches the object's surface again. The above cycle is repeated to trace the object contour until the robotic finger returns to the designed trajectory.

5.3. Object manipulation

If slippage occurs between a finger and an object, the robotic hand cannot manipulate the object without any control based on acquired slippage information. In object manipulation tests, we verified its capability to acquire slippage information using one-finger manipulation.

The robotic finger moves the parallelepiped object that is put on the acrylic table (Fig. 6). During this manipulation, if the time derivative of the shearing force caused on the tactile sensor exceeds a specified threshold, slippage is assumed, and the finger moves slightly downward to increase compressive force. Since the sensing element is made of silicone rubber, friction between the finger and the object can be increased without greatly increasing friction between the object and the table.

In this experiment, the robotic finger moves along a rectangular trajectory, and its movement is measured by a position sensitive detector (PSD; PS1100, Toyonaka Kenkyusyo, Co.).

6. Experimental Results and Discussion

6.1. Scanning on flat surface

First, Fig. 7 shows variations in normal force, shearing force, and friction coefficient obtained during scanning to examine the dynamic characteristics of the tactile sensor. It also shows the case of 1-μm and 6.2 mm/sec.

Shearing force starts at zero because it is not applied at zero speed. After the start, it abruptly increases to reach a constant value. Normal force shows almost a constant value. The coefficient of friction shows almost a constant value except near the origin. The mean value of the friction

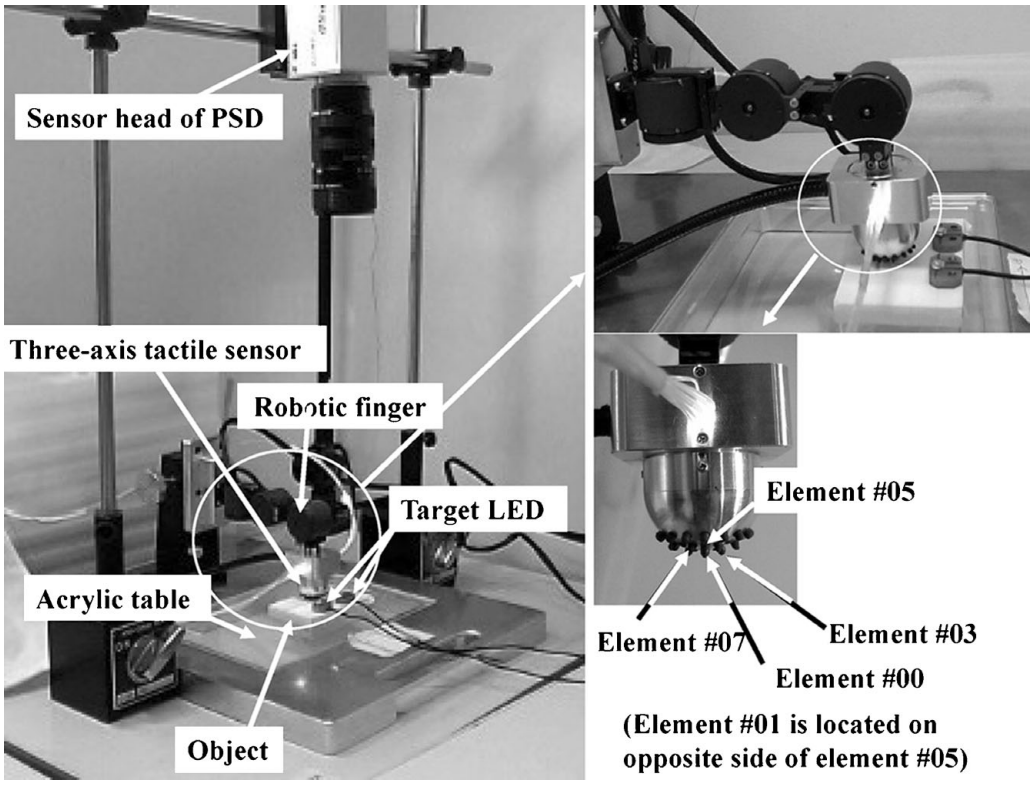

Fig. 6. Object manipulation.

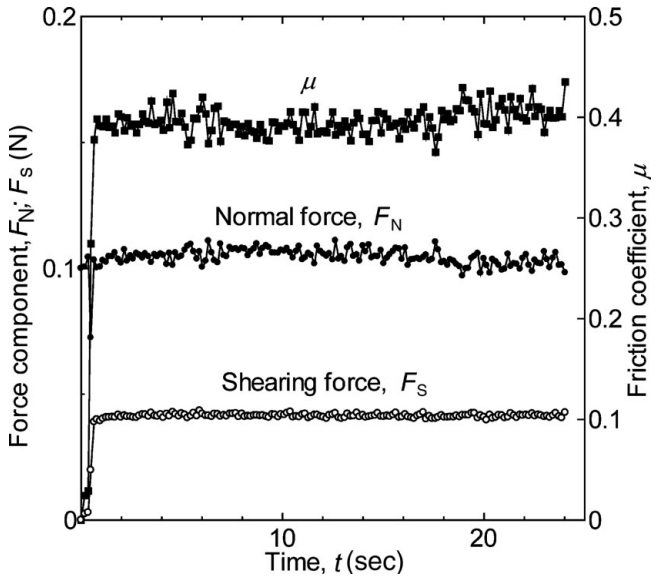

Fig. 7. Variation in force components and friction coefficient during scanning test (1-μm abrasive paper and velocity of 6.2 mm/sec).

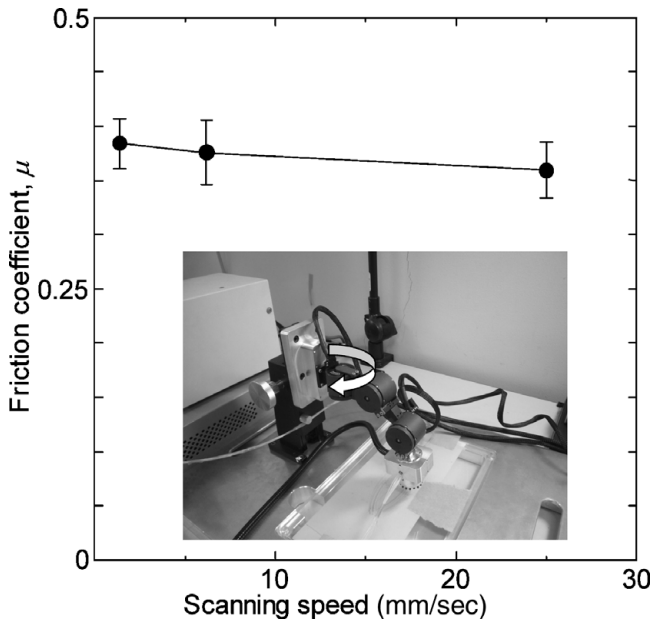

Fig. 8. Dependence of friction coefficient on scanning velocity.

coefficient is 0.39. Friction coefficients for 30- and 60-μm abrasive paper are 0.40 and 0.53, respectively.

Next, variation in friction coefficient against variation in scanning velocity is shown in Fig. 8. 1-μm abrasive paper was adopted as a specimen, and eight trials were performed for each scanning speed. Variation in friction coefficient decreased slightly with an increase of scanning velocity. Since cutting resistance decreased with an increase of cutting speed in grinding theory, we assume that this effect will arise in our experiment.

6.2. Contour tracing

Contour-tracing tests for cylindrical and parallelepiped objects are shown in Figs. 9 and 10, respectively. Maximum deviation from the desired trajectory is about 3.6 mm in Fig. 9. The disconnected portion on the trajectory is caused by the searching process. Based on the present program, since the finger's motion is limited to the x- or y-direction for programming simplicity, tangential touching causes lost contour trajectory. At that time, the robotic finger searches the contour by a small square of trajectory 10 times 10 mm until

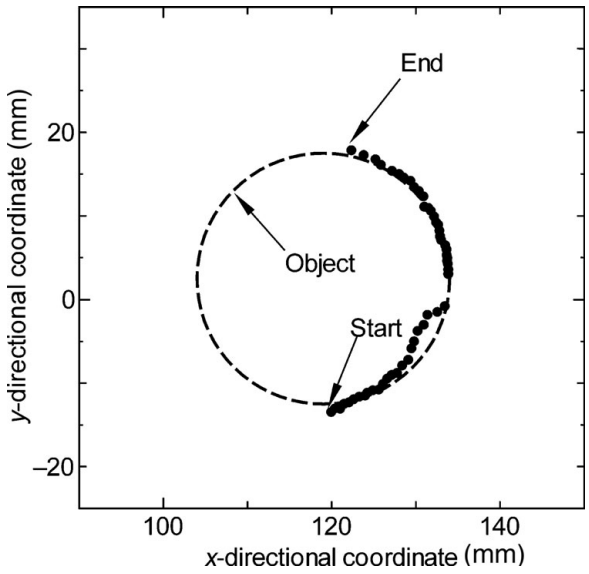

Fig. 9. Contour tracing for cylindrical surface.

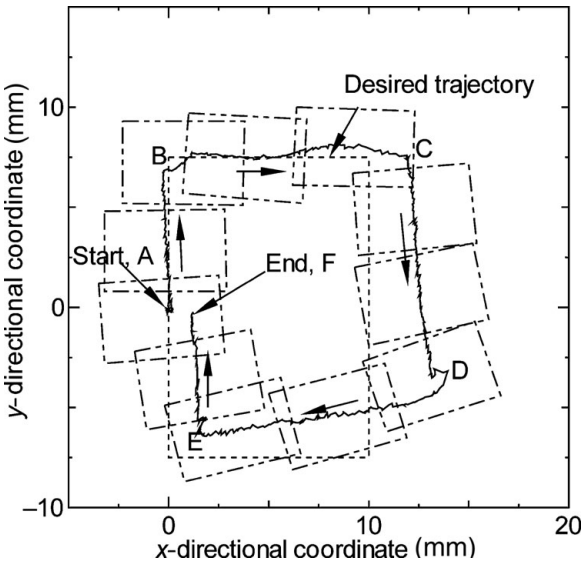

Fig. 11. Manipulation of parallelepiped object.

it finds the contour again. Except for the above deviation and the disconnected portion, the robotic finger traces the cylinder's contour.

On the other hand, since the parallelepiped object's contour is composed of straight lines, exploring precision is higher than for the cylinder. However, since it has corners, it loses the contour at the corner. Except for the corners, the maximum deviation from the contour is 2.7 mm.

6.3. Object manipulation

Figure 11 shows the trajectory and attitude of the manipulated object. To simplify seeing the attitude, the parallelepiped object is shown as 1/10 size in Fig. 12. As shown in Fig. 11, the object moves along the desired trajectory with considerable deviation. To analyze the slippage phenomenon, variations in normal and shearing force derivatives are shown in Fig. 12. In this experiment, since sensor elements #00 and #07 emit rather large signals compared to elements #01, #03, and #05, which touch the surface, their variations are shown in Fig. 12. Such elements as #00, #01, #3, and #05 are shown in Fig. 6. To show the relationship between the representative points of Figs. 11 and 12, corresponding points are shown in both figures as identical characters. For our controller, the absolute time derivative of the shearing force is compared to a threshold. Two horizontal solid lines at a value of −0.06 and 0.06 N/s in Fig. 12 show the threshold of shearing force derivative. If the time derivative of shearing force derivative exceeds the band sandwiched by these two horizontal lines, the controller registers that slippage has occurred.

In this experiment, since finger moving starts when the compressive force exceeds 0.5 N at point A, normal force abruptly decreases just after point A in terms of the inclination of the sensing element. Since the present robotic finger only possesses 3-degrees of freedom and cannot control its inclination, the contact point is changed. Consequently, just after point B's normal force of element #00 decreases, the normal force of element #07 increases.

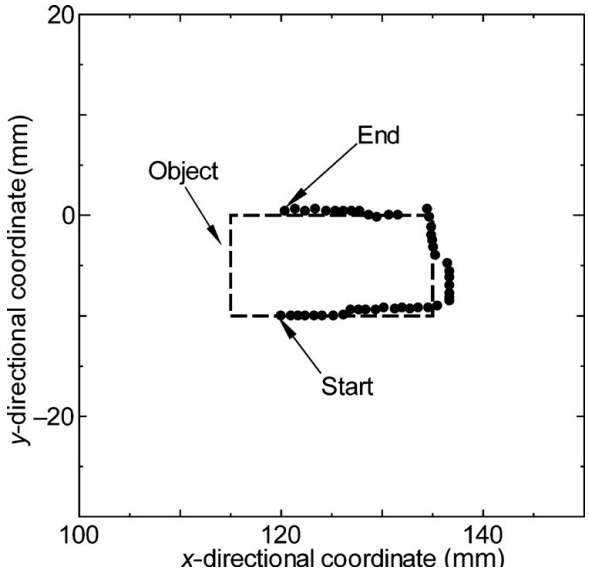

Fig. 10. Contour tracing for parallelepiped surface.

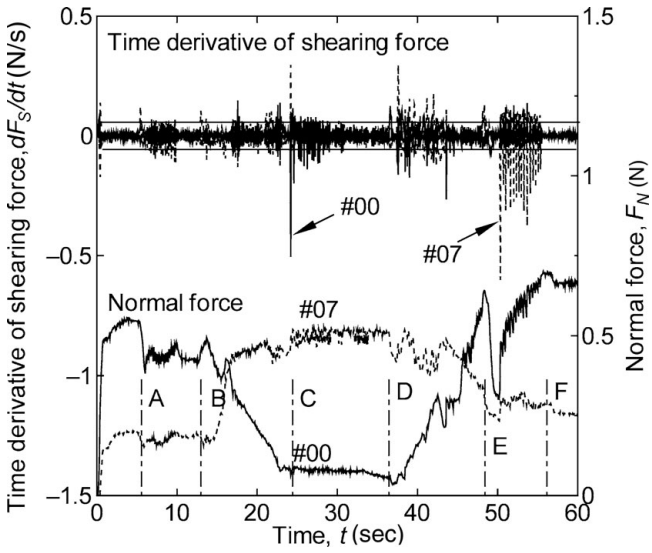

Fig. 12. Time derivative of shearing force in object manipulation.

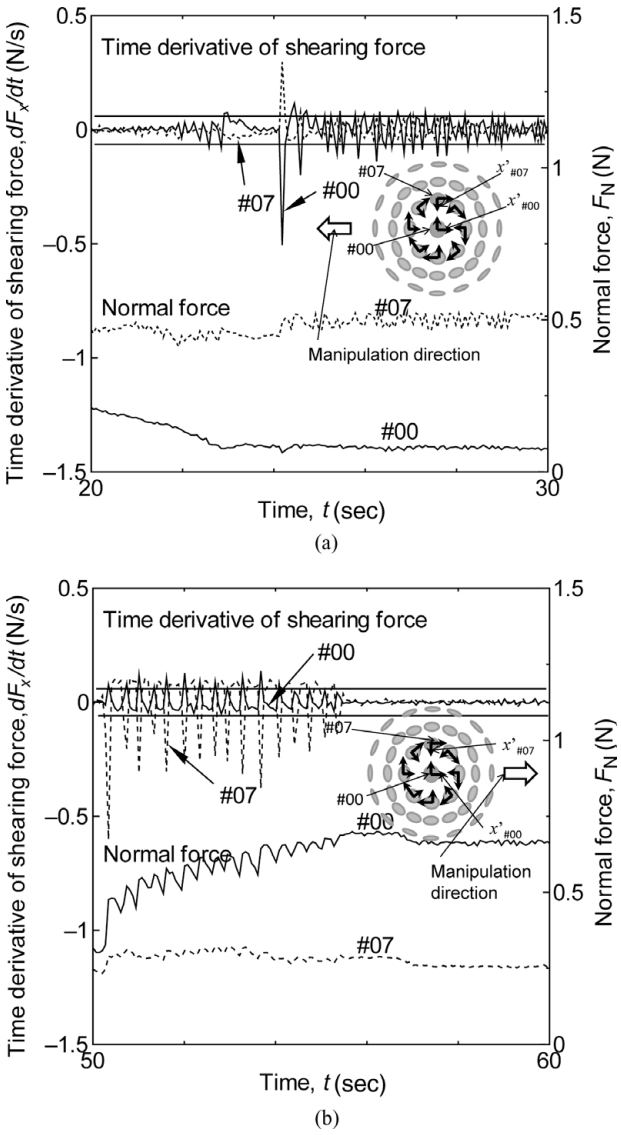

Fig. 13. Detail variation in time derivative of shearing and normal forces (a) Near point C (b) Near point E.

Next, we examine the time derivative of the shearing force in Fig. 12. If the derivative vibration is examined on the segments, the derivative on BC, CD, DE, and EF is larger than on AB. This result means that slippage on BC, CD, DE, and EF is more considerable than on AB. Consequently, deviation after point C in Fig. 11 becomes considerable in terms of slippage.

To examine the above variations in normal force and the time derivative of the shearing force, their details are shown in Fig. 13(a) and (b), which are around points C and E, respectively. In order to depict the location of sensing element, the local coordinates of sensing elements #00 and #07 and manipulation direction are shown in Fig. 13. Since manipulation direction of Fig. 13 (a) is opposite from that of Fig. 13(b), detected time derivative of shearing force is reversed between Fig. 13(a) and (b).

The finger control program regulates the fingertip velocity, not the force. Based on the finger control program, if the absolute time derivative of the shearing force exceeds an appropriate threshold (0.06 N/s in the present paper), z-directional velocity is determined to be 2 mm/sec during the absolute time derivative of the shearing force that exceeds the threshold to enhance the contact force between the sensor tips and the object. For Fig. 13(a), a salient peak of the time derivative of the shearing force is observed around $t = 24$ sec. Although the finger control program recognizes slippage due to the salient peak, normal force apparently does not increase because of the sole peak.

On the other hand, time derivatives of the shearing force of #00 and #07 show bumpy variation including several peaks in Fig. 13(b) to increase periodically the normal force of #00. The normal force of pin #07 does not increase despite the peaks occurring at pin #07. Although it seems strange, the following is reasonable: since four pins around pin #00 are touching the object, and pin #07 is one of the four pins (#01, #03, #05, and #07), the result of Fig. 13(b) shows that slippage occurs in the periphery of the contact area. Since our robotic finger does not have six joints but three joints, it cannot control fingertip attitude. The fingertip touches the target at an angle almost perpendicular angle to the table on EF, while it cannot keep the perpendicular angle on CD. Therefore, the normal force of #00 increases on EF because element #00 is located at the sensor vertex.

The above three experimental results show that the present robotic finger possesses sufficient sensing ability to acquire the friction coefficients of the object surface, its contour, and the slippage phenomenon; these are useful bits of information for a multifingered hand. Since a mechanism for modifying object movement from the deviation in terms of feedback is presently not incorporated into the finger control program, our program must be improved in the future.

7. Conclusion

In the present paper, a three-axis tactile sensor was mounted on a robotic finger of 3-degrees of freedom to evaluate the tactile sensor for dexterous hands. A series of three kinds of experiments was performed. First, the robotic hand touched and scanned flat specimens to evaluate their friction coefficient. Second, it detected the contours of parallelepiped and cylindrical objects. Finally, it manipulated a parallelepiped object put on a table by sliding it. Since the present robotic hand performed the above three tasks, we believe that the hand is applicable to dexterous hands in subsequent studies.

Acknowledgment

This study was supported by fiscal 2006 grants from the Ministry of Education, Culture, Sports, Science, and Technology (Grant-in-Aid for Scientific Research, No. 18656079).

References

1. H. M. Raibert and J. E. Tanner "Design and implementation of a VSLI tactile sensing computer," *Int. J. Robotics Res.* **1**(3), 3–18 (1982).
2. S. Hackwood, G. Beni, L. A. Hornak, R. Wolfe and T. J. Nelson, "Torque-sensitive tactile array for robotics," *Int. J. Robotics Res.* **2**(2), 46–50 (1983).

3. P. Dario, D. D. Rossi, C. Domenci and R. Francesconi, "Ferroelectric Polymer Tactile Sensors With Anthropomorphic Features," *Proceedings of the 1984 IEEE International Conference on Robotics and Automation* (1984) pp. 332–340.
4. J. L. Novak, "Initial Design and Analysis of a Capacitive Sensor for Shear and Normal Force Measurement," *Proceedings of the 1989 IEEE International Conference on Robotic and Automation* (1989) pp. 137–145.
5. H. R. Nicholls and M. H. Lee, "A survey of robot tactile sensing technology," *Int. J. Robotics Res.* **8**(3), 3–30 (1989).
6. M. Ohka, M. Kobayashi, T. Shinokura and S. Sagisawa, "Tactile expert system using a parallel-fingered hand fitted with three-axis tactile sensors," *JSME Int. J., Series C* **37**(1), pp. 138–146 (1994).
7. S. Takeuchi, M. Ohka and Y. Mitsuya, "Tactile Recognition Using Fuzzy Production Rules and Fuzzy Relations for Processing Image Data from Three-dimensional Tactile Sensors Mounted on a Robot Hand," *Proceedings of the Asian Control Conference*, Vol. 3 (1994) pp. 631–634.
8. H. Mott, M. H. Lee and H. R. Nicholls, "An Experimental Very-High-Resolution Tactile Sensor Array," *Proceedings of the 4th International Conference on Robot Vision and Sensory Control* (1984) pp. 241–250.
9. K. Tanie, K. Komoriya, M. Kaneko, S. Tachi and A. Fujiwara, "A High-Resolution Tactile Sensor Array," **In**: *Robot Sensors Vol. 2: Tactile and Non-Vision* (IFS, Kempston, UK, 1986) pp. 189–198.
10. H. R. Nicholls, "Tactile Sensing Using an Optical Transduction Method," **In**: *Traditional and Non-traditional Robot Sensors* (T. C. Henderson, ed.) (Springer-Verlag, Berlin Heidelberg, 1990) pp. 83–99.
11. M. Kaneko, H. Maekawa and K. Tanie, "Active Tactile Sensing by Robotic Fingers Based on Minimum-External-Sensor-Realization", *Proceedings of the IEEE International Conference on Robotics and Automation* (1992) pp. 1289–1294.
12. H. Maekawa, K. Tanie, K. Komoriya, M. Kaneko, C. Horiguchi and T. Sugawara, "Development of a Finger-Shaped Tactile Sensor and Its Evaluation by Active Touch," *Proceedings of the 1992 IEEE International Conference on Robotics and Automation* (1992) pp. 1327–1334.
13. M. Ohka, Y. Mitsuya, Y. Matsunaga and S. Takeuchi, "Sensing Characteristics of an optical three-axis tactile sensor under combined loading," *Robotica* **22**, 213–221 (2004).
14. M. Ohka, T. Kawamura, T. Itahashi, T. Miyaoka and Y. Mitsuya, "A tactile recognition system mimicking human mechanism for recognizing surface roughness," *JSME Int. J., Series C*. **48**(2), pp. 278–285 (2005).
15. M. Ohka, H. Kobayashi and Y. Mitsuya, "Sensing Characteristics of an Optical Three-axis Tactile Sensor Mounted on a Multi-fingered Robotic Hand," *IEEE/RSJ International Conference on Intelligent Robots and Systems* (2005) pp. 1959–1964.
16. M. Ohka, H. Kobayashi, J. Takata and Y. Mitsuya, "Sensing Precision of an Optical Three-axis Tactile Sensor for a Robotic Finger," *Proceedings of the ROMAN 2006-The 15th IEEE International Symposium on Robot and Human Interactive Communication* (2006) pp. 214–219.
17. H. Yussof, M. Ohka, H. Kobayashi, J. Takata, M. Yamano and Y. Nasu, "Development of an optical three-axis tactile sensor for object handling tasks in humanoid robotic systems", *Studies in Computational Intelligence* **76**, 43–51 (2007).
18. D. E. Whitney, "Resolved motion rate control of manipulators and human prostheses," *IEEE Trans. Man Mach. Syst.* **10**(2), 47–53 (1969).
19. P. Muir and C. P. Neuman, "Resolved Motion Rate and Resolved Acceleration Servo-Control of Wheeled Mobile Robots," *Proceedings of the 1990 IEEE International Conference on Robotics and Automation* Vol. 2 (1990), pp. 1133–1140.